

REPORT



Development and pharmacokinetic assessment of a fully canine anti-PD-1 monoclonal antibody for comparative translational research in dogs with spontaneous tumors

Sho Yoshimoto^{a*}, Nicholas Chester^{b*,†}, Ailian Xiong^a, Enrico Radaelli^c, Hong Wang^b, Marc Brillantes^b, Gayathri Gulendran^d, Patrick Glassman^e, Don L. Siegel^{d,f}, and Nicola J. Mason^{id a,c,d}

^aDepartment of Clinical Sciences and Advanced Medicine, School of Veterinary Medicine, University of Pennsylvania, Philadelphia, PA, USA;

^bVetigenics LLC, B-Labs, Cira Center, Philadelphia, PA, USA; ^cDepartment of Pathobiology, School of Veterinary Medicine, University of Pennsylvania, Philadelphia, PA, USA; ^dCenter for Cellular Immunotherapies, Perelman School of Medicine, University of Pennsylvania, Philadelphia, PA, USA;

^eDepartment of Pharmaceutical Sciences, Temple University School of Pharmacy, Philadelphia, PA, USA; ^fDepartment of Pathology and Laboratory Medicine, Perelman School of Medicine, University of Pennsylvania, Philadelphia, PA, USA

ABSTRACT

PD-1 checkpoint inhibitors have revolutionized the treatment of patients with different cancer histologies including melanoma, renal cell carcinoma, and non-small cell lung carcinoma. However, only a subset of patients show a dramatic clinical response to treatment. Despite intense biomarker discovery efforts, no single robust, prognostic correlation has emerged as a valid outcome predictor. Immune competent, pet dogs develop spontaneous tumors that share similar features to human cancers including chromosome aberrations, molecular subtypes, immune signatures, tumor heterogeneity, metastatic behavior, and chemotherapeutic response. As such, they represent a valuable parallel patient population in which to investigate predictive biomarkers of checkpoint inhibition. However, the lack of a validated, non-immunogenic, canine anti-PD-1 antibody for pre-clinical use hinders this comparative approach and prevents potential clinical benefits of PD-1 blockade being realized in the veterinary clinic. To address this, fully canine single-chain variable fragments (scFvs) that bind canine (c)PD-1 were isolated from a comprehensive canine scFv phage display library. Lead candidates were identified that bound with high affinity to cPD-1 and inhibited its interaction with canine PD-L1 (cPD-L1). The lead scFv candidate re-formatted into a fully canine IgG_D reversed the inhibitory effects of cPD-1:cPD-L1 interaction on canine chimeric antigen receptor (CAR) T cell function. In vivo administration showed no toxicity and revealed favorable pharmacokinetics for a reasonable dosing schedule. These results pave the way for clinical trials with anti-cPD-1 in canine cancer patients to investigate predictive biomarkers and combination regimens to inform human clinical trials and bring a promising checkpoint inhibitor into the veterinary armamentarium.

ARTICLE HISTORY

Received 11 July 2023
Revised 31 October 2023
Accepted 20 November 2023

KEYWORDS



Canine; checkpoint inhibitor; monoclonal antibody; PD-1; pharmacokinetics

Introduction

Programmed cell death protein 1 (PD-1 or CD279) is a co-inhibitory checkpoint molecule expressed primarily on the surface of activated T cells, NK cells, and B cells. Interaction of PD-1 with its primary ligand PD-L1, expressed on macrophages, DCs, and other stromal cells inhibits CD4⁺ and CD8⁺ T cell effector functions, including proliferation, cytotoxic activity, cytokine secretion, and migration.¹ As such, PD-1:PD-L1 interactions protect the host from over-exuberant immune responses. This important negative regulatory function of the PD-1:PD-L1 interaction is underscored by the development of severe autoimmunity in PD-1 deficient mouse strains.² PD-L1 is also expressed on tumor cells, tumor-associated macrophages, and cancer-associated fibroblasts, and its expression is strongly up-regulated by inflammatory


cytokines including IFN- γ and TNF- α produced by T cells.³ Therefore, activated PD-1⁺ tumor-specific T cells contribute to the expression of PD-L1 in the tumor microenvironment, which drives tumor-specific T cell exhaustion and significantly impairs anti-tumor immune responses.

Blockade of the PD-1:PD-L1 interaction with anti-PD-1 or anti-PD-L1 antibodies enhances anti-tumor immunity and has led to an increase in tumor infiltrating lymphocytes (TILs) and impressive clinical responses in a subset of human patients with different tumor histologies including malignant melanoma, non-small cell lung carcinoma, and renal cell carcinoma.^{4–6} However, durable clinical responses are only observed in 20–30% of the patients treated with anti-PD-1 or anti-PD-L1 antibodies, leading to intense efforts to understand the mechanisms of resistance and to identify correlative biomarkers of response that may streamline patients to immune

CONTACT Nicola J. Mason  nmason@vet.upenn.edu  Department of Clinical Sciences and Advanced Medicine, School of Veterinary Medicine, University of Pennsylvania, Room 315, Hill Pavilion, 380 South University Avenue, Philadelphia, PA 19104, USA

*These authors contributed equally to the manuscript.

†Deceased, March 19th, 2022.

 Supplemental data for this article can be accessed online at <https://doi.org/10.1080/19420862.2023.2287250>.

© 2023 The Author(s). Published with license by Taylor & Francis Group, LLC.

This is an Open Access article distributed under the terms of the Creative Commons Attribution-NonCommercial License (<http://creativecommons.org/licenses/by-nc/4.0/>), which permits unrestricted non-commercial use, distribution, and reproduction in any medium, provided the original work is properly cited. The terms on which this article has been published allow the posting of the Accepted Manuscript in a repository by the author(s) or with their consent.

checkpoint inhibitor (ICI) monotherapy or to alternative therapeutic strategies.⁷ Tumor mutational burden (TMB), IFN- γ response signatures, microsatellite instability-high/mismatch repair deficiency (MSI-H/MMRD), and expression of PD-L1 on tumor cells and tumor infiltrating immune cells have shown predictive value in clinical response to anti-PD-1 therapy in different cancer histologies.^{8,9} Strategies that combine anti-PD-1 and anti-PD-L1 monoclonal antibodies (mAbs) with other ICIs such as anti-CTLA4, anti-TIM-3, anti-TIGIT, and anti-Lag3 antibodies, or with the administration of cancer vaccines, chimeric antigen receptor (CAR)-T cell therapies, radiation, chemotherapy, and small molecule inhibitors to augment anti-tumor activity are under active investigation.

In veterinary medicine, the use of checkpoint inhibitors is in its infancy principally due to the lack of fully canine mAbs with favorable pharmacokinetic/pharmacodynamic properties that can be produced economically at clinical scale. Furthermore, TMB, which correlates with clinical response to checkpoint inhibition in some cancer types in humans, is generally lower in canine tumors compared to human tumors¹⁰. As such, the efficacy of ICI as monotherapies remains to be proven in veterinary medicine and their use in combination with radiation therapy, chemotherapy, vaccines, genetically engineered immune cells, and other immunotherapies to enhance their effectiveness and provide significant clinical benefit requires investigation.

Here, the development and validation of a fully canine, anti-cPD-1 antibody derived from a canine single-chain variable fragment (scFv) phage display library is described. The antibody demonstrated favorable *in vivo* safety, tolerability, and pharmacokinetic profiles and was produced at high yield enabling scale-up for clinical use. Development of this antibody now enables investigation of anti-PD-1 therapy to promote anti-tumor immunity in dogs with immune responsive cancers. It also provides an important comparative tool to investigate relative biomarkers of response and mechanisms of resistance to PD-1 checkpoint inhibition in immune competent pet dogs that may be valuable to inform human clinical trial design.

Results

Isolation of canine PD-1 specific scFv clones

Canine anti-cPD-1 scFvs were isolated from a previously constructed 40-billion member canine IgM/IgG/ λ / κ scFv phage display library built from canine B cell mRNA. mRNA was isolated from discarded splenic material of seven otherwise healthy dogs that had undergone therapeutic splenectomy for benign conditions. The construction of the library used the pComb3X phagemid vector and protocols as described¹¹ with a set of oligonucleotide primers designed to capture transcripts encoded by all canine immunoglobulin heavy and light-chain germline genes as listed in the IMGT database.¹² A total of over 1,000 individual RT/PCR reactions for VH- γ , VH- μ , V κ , and V λ had been carried out (145 reactions per spleen) and amplification products were recombined using strand-overlap-extension to generate four independent libraries comprising VH- γ gene segments paired with V κ and V λ gene segments and VH- μ gene segments paired with V κ and V λ gene segments. After ligation into pComb3X, electroporations into

E. coli were performed to generate over 40 billion independent bacterial transformations. To assure the quality of the library, successful amplification of each of the more than 1,000 heavy and light chain cDNA PCRs was confirmed by agarose gel electrophoresis before incorporation into the library. Analysis of dozens of individual scFv clones from the unselected primary library underwent nucleotide sequencing which showed a nearly 100% presence of complete heavy chain/light chain scFv inserts in all clones and which showed distributions of heavy and light-chain immunoglobulin gene families and their genes and heavy-chain CDR3 lengths similar to those found from analysis of peripheral blood canine immune repertoires.^{13–16} This canine scFv phage display library has been used in several dozen panning campaigns to isolate canine antibodies of therapeutic interest including anti-canine CTLA-4 antibodies as previously described.¹⁷ To select anti-cPD-1 scFvs from the phage display library, recombinant cPD-1 was directly coated onto the wells of a microtiter plate and used as the target antigen. An aliquot of the pooled VH- γ /V κ , VH- γ /V λ , VH- μ /V κ , and VH- μ /V λ canine scFv library underwent four rounds of solid-phase selection (“panning”) against the immobilized cPD-1 as previously described.¹⁸ To verify that the selected phage contained cPD-1-specific scFv phage particles, polyclonal scFv phage from each round of panning was evaluated by phage ELISA against cPD-1 (Figure 1).¹⁹ Marked enrichment of the library for cPD-1 binding scFv-expressing phage was observed in the third round of panning (P3) and increased in the fourth round of panning (P4). Binding was specific to cPD-1 as binding to the irrelevant human CD19 target antigen was not observed.

An initial survey of positive cPD-1 binders was performed by examining 16 clones from P3 and 16 clones from P4 for their ability to bind to cPD-1 by monoclonal phage ELISA as previously described.¹⁹ 10/16 clones from P3 and 15/16 clones from P4 bound to cPD-1 (Figure 2A–B). Fourteen unique clones were identified by nucleotide sequencing from these 25 binders. Six comprised λ light chains and eight comprised κ light chains. These 14 clones were produced as soluble scFv fragments and their binding to cPD-1 was assessed in an ELISA by detecting the hemagglutinin (HA) tag on their carboxy terminus (Figure 3A). Six soluble scFvs were shown to bind cPD-1 as a function of plate-bound streptavidin-captured biotinylated cPD-1. Following this initial survey to assess positivity rate, a high-throughput screen of 176 clones (88 from P3 and 88 from P4) was performed. This screen identified an additional eight unique scFv clones (data not shown). Five of these eight clones produced well as soluble scFv, and their ability to specifically bind cPD-1 was confirmed by ELISA (Figure 3B).

Assessment of blocking capacity of cPD-1 scFv clones

Based on the results of soluble scFv binding to cPD-1, nine clones that bound cPD-1 (3–4, 3–8, 3–13, 4–2, 4–9, 4–14, P4B1, P3C6, and P4F3) and two clones that showed minimal binding (P4F8 and P4C1) were selected and assessed for their ability to inhibit the interaction of soluble cPD-1 with cPD-L1-Fc at three molar ratios of scFv to cPD-L1-Fc (70:1, 23:1, and 7:1, respectively). Briefly, a fixed concentration of biotinylated cPD-1 (30 nM) was incubated with increasing concentrations of cPD-L1

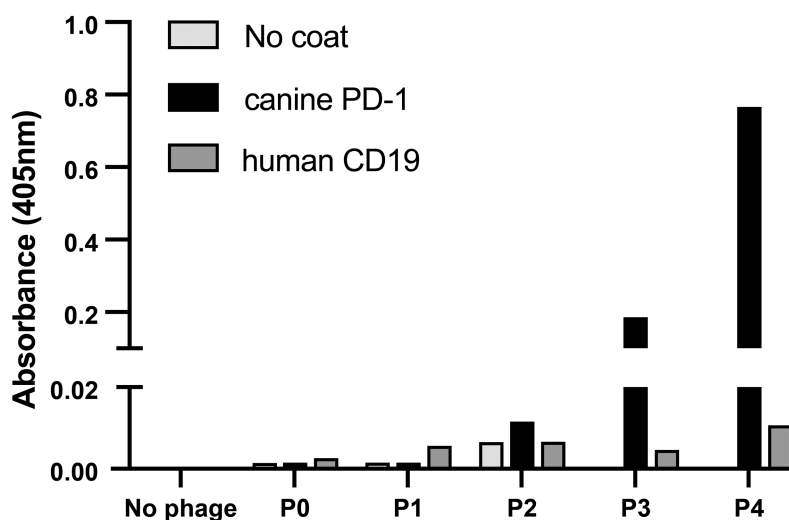


Figure 1. Enrichment of canine scFv phage display library after panning against cPD-1 antigen. Recombinant cPD-1 was adsorbed to a microtiter plate overnight at 4°C. Wells were washed and blocked with 2% milk in PBS (MPBS) for 1 hour at 37°C. Initial unpanned library (P0) and libraries of phage obtained after each round of selection (P1 through P4) were added to coated plates and incubated for 1 hour at 37°C. Plates were washed with PBS supplemented with 0.1% Tween (PBST) and bound phage was detected using a 1:5000 dilution of HRP-conjugated anti-M13 mAb in MPBS. Bound phage were detected with ABTS. OD was read at 405 nm after 30 min using a Molecular Devices SpectraMax 340 spectrophotometer.

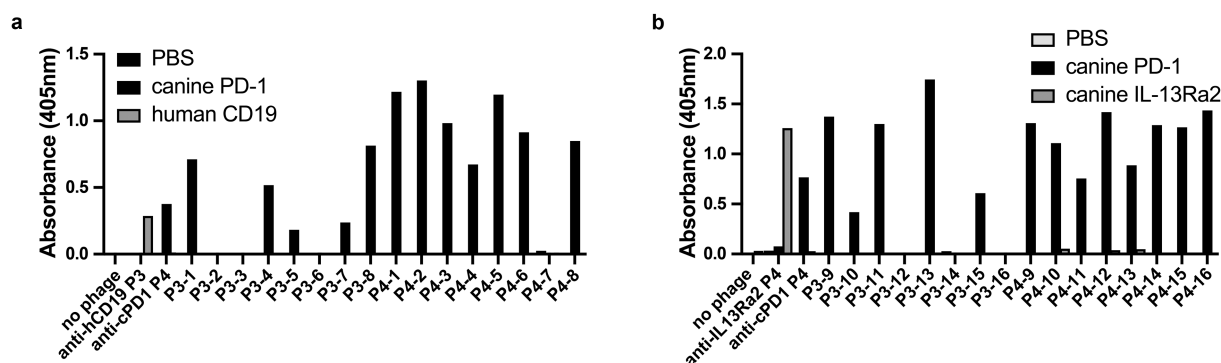


Figure 2. Binding of randomly selected scFv-expressing monoclonal phage clones from panning rounds 3 and 4 to cPD-1. ELISA plates were coated with recombinant cPD-1 and human CD19 (left) or canine IL-13Ra2 (right) as controls. Polyclonal phage from the fourth round of panning against cPD-1 served as positive control phage on both plates. Polyclonal phage from the third round of panning against human CD19 (left graph) and fourth round of panning against canine IL-13Ra2 (right graph) (both sets of phage from unrelated projects) served as positive phage controls. Each monoclonal phage was screened once for binding to cPD-1.

-Fc (10, 20, or 100 nM) either alone or in the presence of a fixed concentration of cPD-1 specific scFvs (700 nM). Biotinylated cPD-1:cPD-L1-Fc complexes were captured onto a streptavidin coated plate and then detected using an anti-Fc antibody. In the absence of cPD-1 specific scFvs blocking the cPD-1:cPD-L1 interaction, complex formation and detection would occur. However, if a cPD-1 specific scFv inhibits cPD-1 binding to cPD-L1-Fc, a reduced or complete lack of signal would be the read out in this assay (Figure 4A). With the exception of clones 3–8, 4–2, and 4–9, all clones exhibited a degree of dose-dependent inhibition of cPD-1 binding to cPD-L1 (Figure 4B and data not shown). However, only clone P3C6 completely inhibited cPD-1 binding to cPD-L1 at each of the three cPD-L1 concentrations used in the assay.

Selected cPD-1 specific clones bind to cell surface cPD-1

To determine whether selected cPD-1 clones bind to cPD-1 expressed on the cell surface, the human erythroleukemic cell line K562, previously edited to remove the FcγRII (CD32;

KTδ32), was engineered to express cPD-1 using a retroviral vector carrying a puromycin selection cassette (KTδ32.cPD-1), and KTδ32.cPD-1 cells were selected in puromycin. Four HA-tagged soluble scFvs that inhibited cPD-1:cPD-L1 binding were incubated with either KTδ32 or KTδ32.cPD-1 cells, and binding was determined by flow cytometry (Figure 5). An anti-MERS scFv and clone 3–7 (shown not to bind soluble cPD-1) were included as negative controls. Clone P3C6 was found to strongly bind to KTδ32.cPD-1 cells, whereas all other clones tested showed much weaker binding or no binding (clone 3–8). Based on cell binding and cPD-1:cPD-L1 inhibitory capability, clones P3C6 and P4B1 were selected for re-formatting as full-length canine IgG_D (analogous to human IgG4) molecules. IgG_D was selected as the IgG subtype on account of its lack of mediating antibody dependent cellular cytotoxicity (ADCC) and complement fixation. Neither of these effector functions is desirable in an anti-PD1 checkpoint inhibitor, and the IgG_D subtype is consistent with the IgG4 subtype of the anti-PD-1 antibodies that are used in the human clinic (e.g., pembrolizumab and nivolumab).

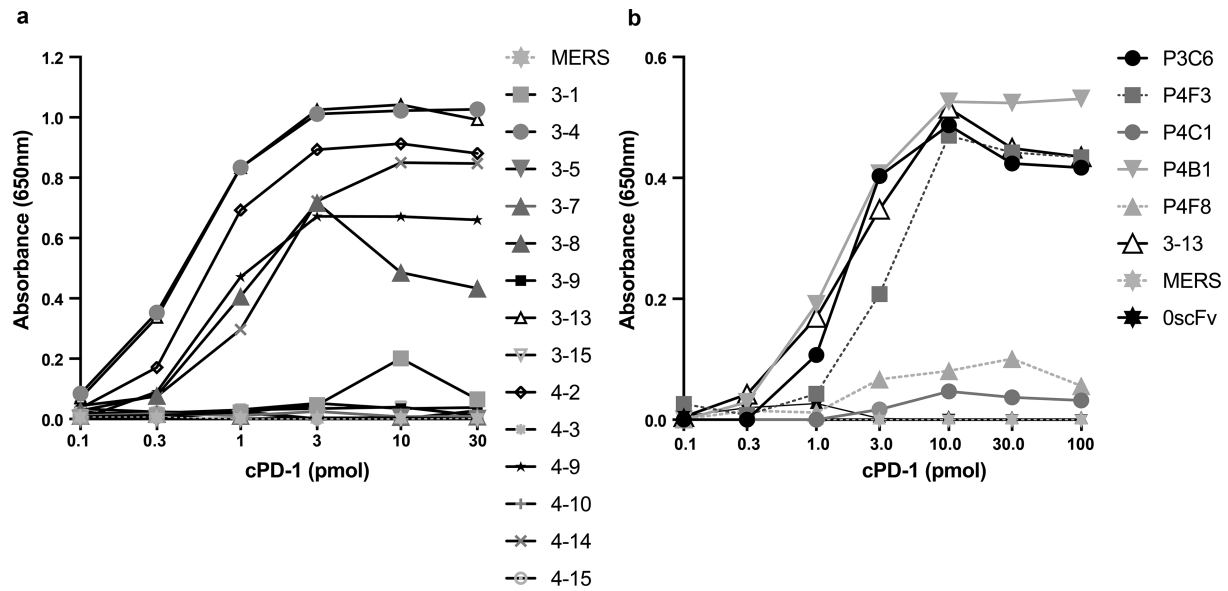


Figure 3. The ability of unique soluble scFv clones to bind to cPD-1 by ELISA. 19 unique soluble scFvs were tested for binding to cPD-1 by ELISA. Increasing amounts of biotinylated cPD-1 were added to streptavidin coated ELISA plate wells and incubated for 1 hour. 0.25 μ g/ml soluble HA-tagged scFvs were added to the wells and bound scFvs were detected using an AP-conjugated anti-HA antibody. An irrelevant soluble HA-tagged scFv against MERS (Middle Eastern Respiratory Syndrome) virus from an unrelated project was used as a negative control. A. unique clones identified in the initial survey. B. additional unique clones identified via high throughput screen. Evaluation of each unique soluble clone against increasing amounts of biotinylated cPD-1 was performed once.

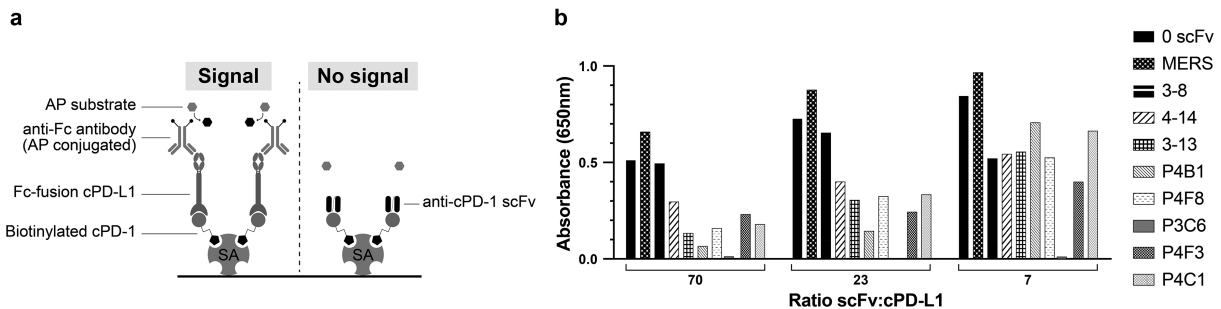


Figure 4. PD-1:PD-L1 inhibition assay. A. Schematic of experimental setup. Soluble biotinylated cPD-1 was incubated with increasing concentrations of cPD-L1-Fc either alone or in the presence of a selected soluble anti-cPD-1 scFv or an irrelevant soluble scFv against Middle Eastern Respiratory Syndrome (MERS) virus. Incubation mixtures were added to ELISA plates pre-coated with streptavidin to capture cPD-1:cPD-L1-Fc complexes. Bound complexes were detected using an anti-Fc-AP conjugate and AP colorimetric substrate. B. soluble anti-cPD-1 scFvs show varying degrees of inhibition of cPD-1 binding to cPD-L1 as revealed by a loss of detectable signal.

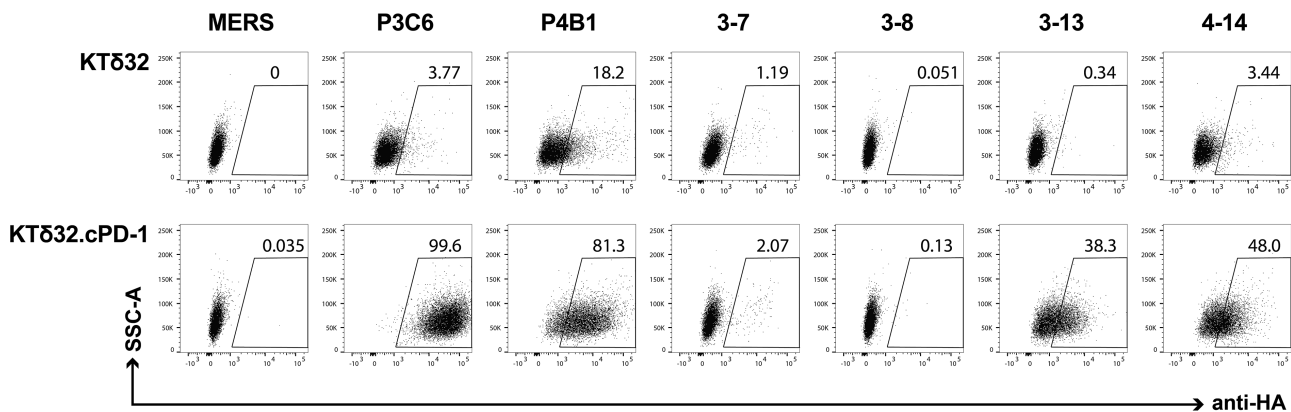


Figure 5. Soluble canine anti-cPD-1 scFv binding to cell surface expressed cPD-1. The human erythroleukemic cell line K562 was gene edited to eliminate the Fc γ RII (CD32) (KT832). Retroviral transduction of edited cells to express cPD-1 was performed, and cPD-1 positive target cells were selected in puromycin. Soluble, purified, HA-tagged scFvs were incubated with target cells, and bound scFvs were detected using a fluorescent anti-HA antibody. The soluble scFv against MERS and scFv 3-7 (negative binders to cPD-1 by ELISA), were used as negative controls.

Heavy chain liabilities are responsible for low yield of P3C6

While P4B1 expressed well as a full-length IgG_D antibody (0.65 µg/µl) from transient transfection of 293T cells, the yield of P3C6 was negligible. Chain swapping experiments with P4B1 confirmed that this liability was associated with the heavy chain of P3C6 (data not shown). Analysis of the heavy chains of P4B1 and P3C6 by IMGT¹² revealed that both were likely encoded by the canine IGHV3–38*01 VH gene and consequently had high sequence homology in their framework regions though their CDRs were different, particularly their CDR3 regions which were of different lengths (Figure 6A, top). P4B1 and P3C6 light chains were very different given that one was a lambda isotype (most likely encoded by the canine germline gene IGLV3–27*01) and the other kappa (most likely encoded by the canine germline gene IGKV3–18*02), respectively (Figure 6A, bottom).

To test whether the expression properties of P4B1 could be conferred to P3C6, we replaced the 11 different heavy-chain framework amino acids in P3C6 with those from P4B1 to create P3C6mut3 (Figure 6A). When paired with the original P3C6 κ light chain, production was improved, but the antibody no longer bound to cPD-1 (data not shown). Strategic back-mutations of seven or six of the 11 P4B1 framework residues to those of P3C6 were carried out to create P3C6mut3.1 and P3C6mut 3.2, respectively (Figure 6A). Paired with the P3C6 κ light chain, both antibodies produced well (P3C6mut3.1: 0.38 µg/µl and P3C6mut3.2: 0.36 µg/µl, respectively, MERS 0.44 µg/µl and P4B1 0.6 µg/µl) and regained PD-1 binding properties similar to the original P3C6 full-length antibody, including binding to cell surface-expressed cPD-1 by flow cytometry (Figure 6B). Because the one difference between P3C6mut3.1 and mut3.2 heavy chains was mut3.1's retention of P3C6's apparent V23M somatic mutation from germline IGHV3–38 that could conceivably contribute to antigen binding or antibody stability, P3C6mut3.1 was selected for further studies.

SPR analyses

The affinity and binding kinetics of P3C6mut3.1 IgG_D to cPD-1 were determined using surface plasmon resonance (SPR). With the HIS-tagged cPD-1 tethered to a CMS chip coated with an anti-HIS antibody and P3C6mut3.1 injected into the flow cell at a constant rate, the on and off rates of P3C6mut3.1 were k_{on} $1.31 \times 10^5 \text{ M}^{-1} \text{ s}^{-1}$ and k_{off} $1.43 \times 10^{-4} \text{ s}^{-1}$ (Fig. S1). The dissociation constant (K_D) of P3C6mut3.1 was 1.1 nM with a binding half-life of 81 min. These binding kinetics are similar to those reported for nivolumab.²⁰ Thus, P3C6mut3.1 displayed a rapid on-rate and slow off-rate, leading to a low single-digit nanomolar affinity. The binding data were fit to a 1:1 binding model which provided a χ^2 value of 25.9 (data not shown).

In vitro functional assessment of P3C6mut3.1 on antigen-specific T cell activity

To determine whether P3C6 mutants were able to reverse the inhibitory effect of cPD-1:cPD-L1 interaction following

antigen-specific T cell activation, canine T cells isolated from a single healthy donor dog, and genetically engineered to express a second-generation CD20 targeting chimeric antigen receptor (CD20 CAR-T cells) were labeled with CTV and co-cultured with irradiated K562 target cells engineered to express canine CD20 without cPD-L1 (K562.cCD20) or with cPD-L1 (K562.cCD20.cPD-L1) (Figure 7A). Expression of cPD-L1 on target K562.cCD20 cells led to inhibition of canine CAR-T cell proliferation as shown by the higher MFI of CTV labeled CAR-T cells co-cultured with K562.cCD20.cPD-L1 (MFI = 2879) compared to K562.cCD20 MFI = 1763 (Figure 7A, B). However, in the presence of P3C6mut3.1 IgG_D mAb, the inhibitory effect of cPD-L1 on CAR-T cell proliferation was reduced (MFI = 2344). Furthermore, the expression of the degranulation marker CD107b by canine CAR-T cells following CD20 antigen engagement was reduced by expression of cPD-L1 on target K562.cCD20.cPD-L1 cells; however, degranulation was almost completely restored in the presence of P3C6mut3.1 IgG_D (Figure 7B, C). Taken together, these data indicate that P3C6mut3.1 can ameliorate the inhibitory effects of cPD-1:cPD-L1 interaction on canine T cells and suggest that it may have therapeutic value in improving anti-tumor T cell mediated immunity *in vivo*.

P3C6mut3.1 identifies cPD-1⁺ lymphocytes in formalin-fixed, paraffin embedded canine lymphoid tissues

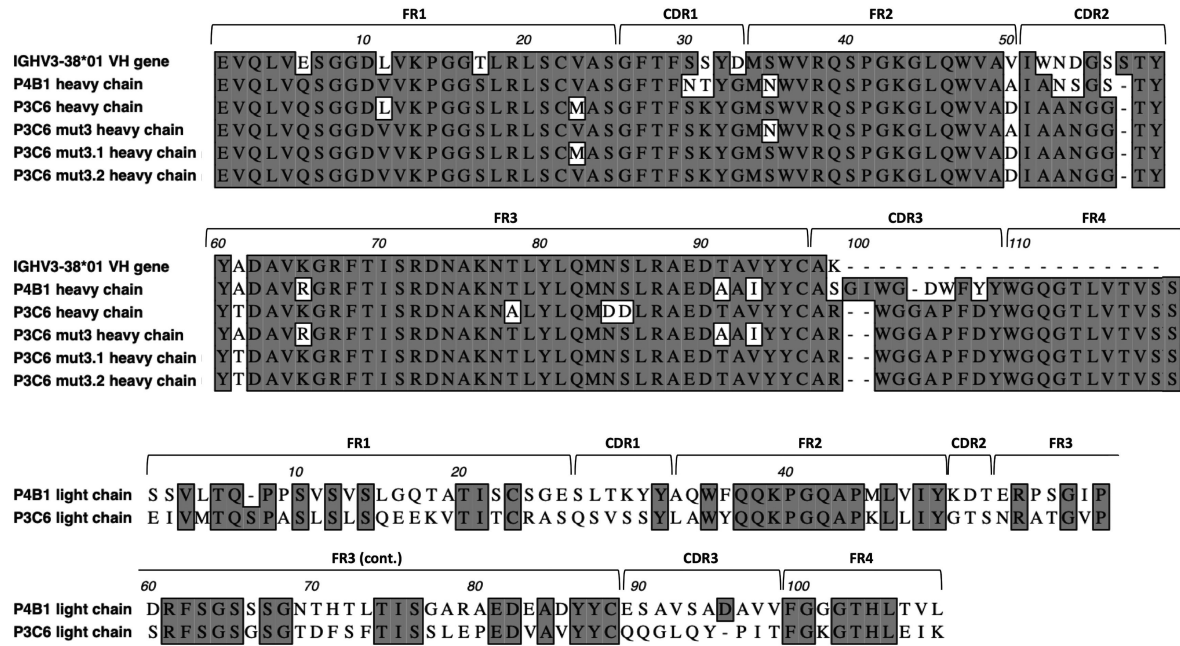
PD-1 is known to be expressed in tumor infiltrating CD8⁺ T cells, other tumor-infiltrating immune cells, and on tumor cells themselves.²¹ However, the exact function of PD-1 on infiltrating immune suppressive cells such as tumor associated macrophages, myeloid cells, T regulatory cells, and tumor cells is controversial. To determine the ability of the P3C6 clone to detect cPD-1 in formalin-fixed, paraffin embedded canine tissues, full-length, HA-tagged P3C6mut3.1 IgG_D was used in immunohistochemical analysis against canine lymph node and 30 other normal FFPE canine tissues in a 40-spot tissue microarray as described in Supplementary Materials and Methods. P3C6mut3.1 was found to intensely stain the membranes of individual lymphocytes in the paracortical zone of the lymph node (Fig. S2), splenic periarteriolar lymphoid sheaths (PALS), and the interfollicular area of the tonsil. No immunolabeling was observed in the sections incubated with the isotype control antibody or where the primary antibody was omitted. Other non-lymphoid tissues included in the TMA were negative for staining with P3C6mut3.1 (data not shown).

Antibody modification and production for in vivo canine studies

Pilot production

The SDS-PAGE analysis of P3C6mut3.1 revealed the presence of half-antibody fragments and heavy-chain dimers (Fig. S3) and a titer of 0.46 mg/ml from a small scale, 100-ml culture. The sequence of P3C6mut3.1 was therefore modified with the IgG_D hinge region (ESTCKCISPCVPESL) replaced by the IgG_B hinge, and two mutations were made in the IgG_B hinge region (ML to

a



b

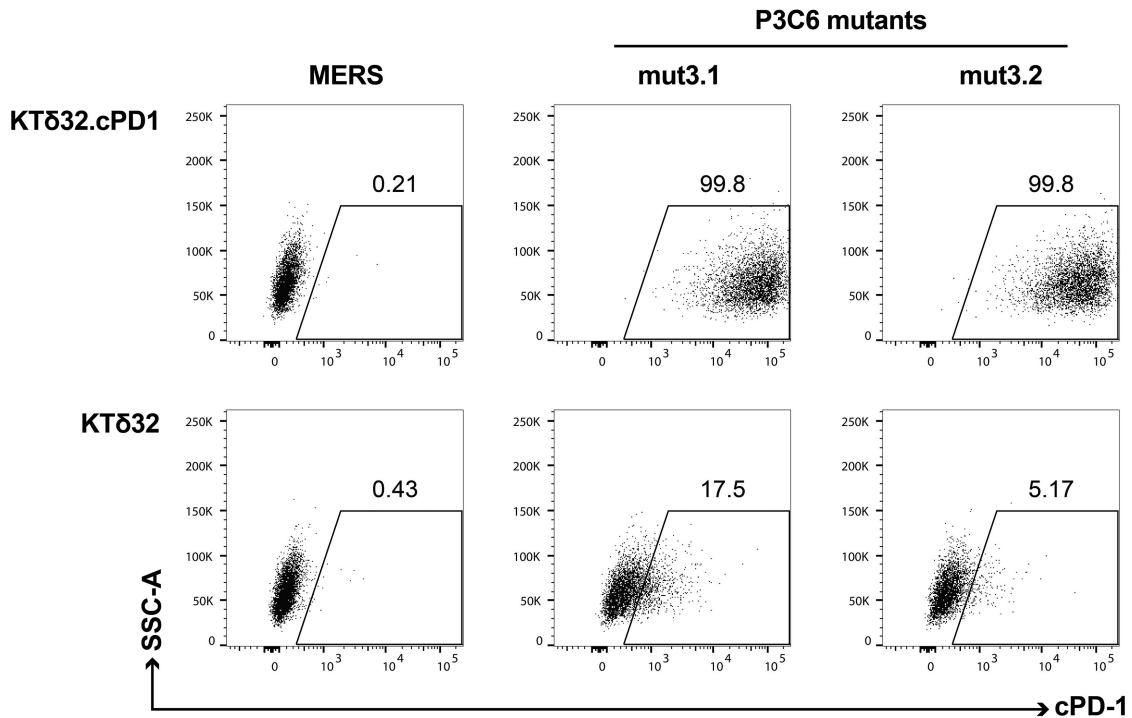


Figure 6. A. Primary structures of lead canine anti-cPD-1 antibodies. A. (top) heavy chain alignments of P4B1, P3C6 and its variants along with canine germline gene IGHV3-38*01. (bottom) light chain alignments of P4B1 and P3C6. Framework and CDR regions use IMGT nomenclature. B. Evaluation of full-length IgG_D (P3C6mut3.1 and mut3.2) canine anti-cPD-1 binding to cell surface-expressed cPD-1 by flow cytometry. Canine IgG_D-HA tagged clones against cPD-1 or the irrelevant MERS antigen (negative control) were used to stain KTδ32 and KTδ32.cPD-1 cells. Bound IgG_D molecules were detected using an anti-HA antibody. Plots are gated on live, 7AAD- cells.

AA) to reduce ADCC (RENGRVPRPPDCPKCPAPEAA). Mutation of the ML amino acids to AA is bolded.

Following sequence confirmation, the hinge modified P3C6mut3.1 (IgG_{D/B}) sequence was transiently transfected into proprietary CHO-K1 cells at a specialized CRO and

expressed in 100-mL culture volume shake flasks. The antibody was purified by Protein A chromatography. SDS-PAGE analysis revealed that the hinge modifications resulted in less half antibody and HC dimer production (Fig. S3) and produced an increase in antibody titer (original sequence: 443 mg/

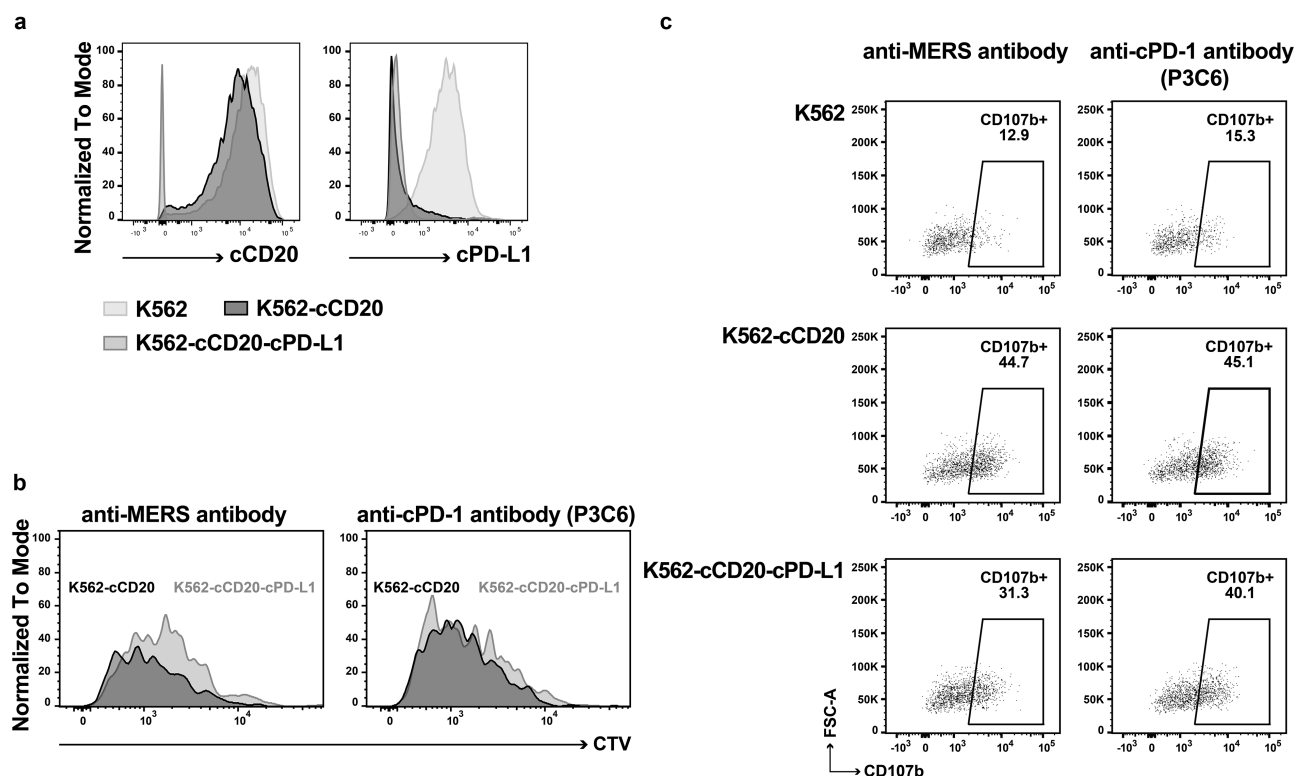


Figure 7. Full-length IgG_D P3C6mut3.1 reverses the effects of PD-L1 inhibition on canine CAR-T cells. **A.** K562 cells were engineered to express canine CD20 (K562-cCD20) and canine PD-L1 (K562-cCD20-cPD-L1) and cell surface expression was confirmed by flow cytometry. **B.** Canine CD20 CAR-T cells from one dog were labeled with cell trace violet (CTV) and co-cultured at an E:T ratio of 1:1 with either K562-cCD20 or K562-cCD20-cPD-L1 in the presence of either anti-MERS or P3C6mut3.1 IgG_D. After 72 hours of culture, proliferation of CD8⁺ CAR-T cells was assessed by flow cytometry. Plots are gated on live CD5⁺ CD8⁺ CAR⁺ cells. **C.** Canine CD20 CAR-T cells from one dog were co-cultured at an E:T ratio of 1:1 with the same target cells as in **A.** Expression of CD107b was determined after 4 hours of co-culture. Plots are gated on live CD5⁺ CD8⁺ CAR⁺ cells.

L; modified sequence: 750 mg/L). Binding of this molecule (IgG_{D/B}) to cPD-1 was confirmed by ELISA (data not shown).

Scale up production

Anti-cPD-1 antibody for *in vivo* use was produced in a single batch using the same proprietary CHO-K1 cells as for pilot production, by the same CRO provider. CHO-K1 cells were transiently transfected with the modified P3C6mut3.1 IgG_{D/B} expression construct, and a 20-L transient production run of the antibody was conducted in shake flasks under appropriate selection pressure. The antibody underwent a one-step purification using Protein A chromatography and the resulting material was analyzed for expression/yield (10.16 mg/mL), endotoxin level (<0.09 EU/mg), and purity by SEC-HPLC (96.03%), SDS-PAGE (reducing and non-reducing), and LC-MS. This material was used for the *in vivo* safety and PK study described below. A summary of the antibody characterization data is shown in Supplemental Table S1.

In vivo pharmacokinetic assessment

As P3C6mut3.1 does not cross react with murine PD-1 (data not shown), pharmacokinetic and biodistribution studies were not performed in mice. To determine the safety, tolerability, and pharmacokinetics (PK, drug exposure) of non-GLP P3C6mut3.1 (IgG_{D/B}) in the target species (dog), a non-terminal, pilot study was performed in four healthy research beagles. There was no vehicle control group. Two adult, intact

males and two adult, intact female dogs were randomly assigned to receive either 2 mg/kg (one male and one female) or 10 mg/kg (one male and one female) P3C6mut3.1 (IgG_{D/B}) (purity 96.12% by SEC-HPLC; endotoxin < 0.08 EU/mg) administered by slow intravenous push once every 3 weeks for a total of two administrations (day 0 and day 21). No pre-medications were given prior to either administration of the antibody. Dogs were monitored for organ-associated toxicities by observations, physical examinations, and hematological and biochemical analyses at the time points indicated in materials and methods. This study was non-terminal, and tissue histopathology was not evaluated. No clinical, hematological, or biochemical adverse events or significant changes in body weight were identified in any of the four dogs treated with two doses of either 2 mg/kg or 10 mg/kg of P3C6mut3.1 (IgG_{D/B}) throughout the 28-day duration of the study (data not shown). Pharmacokinetic analysis revealed biexponential concentration vs. time profiles for both doses of P3C6mut3.1 (IgG_{D/B}) (Figure 8A). Non-compartmental analysis (NCA) was performed to determine individual dog and dose-wise PK parameters (Table 1). There was a trend toward decreasing clearance (CL), increasing volume of distribution (V_{ss}), and increasing half-life (t_{1/2}) at the 10 mg/kg dose compared to the 2 mg/kg dose. This suggests that P3C6mut3.1 (IgG_{D/B}) may have non-linear PK in this dose range, likely due to target-mediated drug disposition (TMDD) as reported for pembrolizumab in human patients.^{22,23} This is supported by the presence of an inflection point between 7 and 20 days, with the

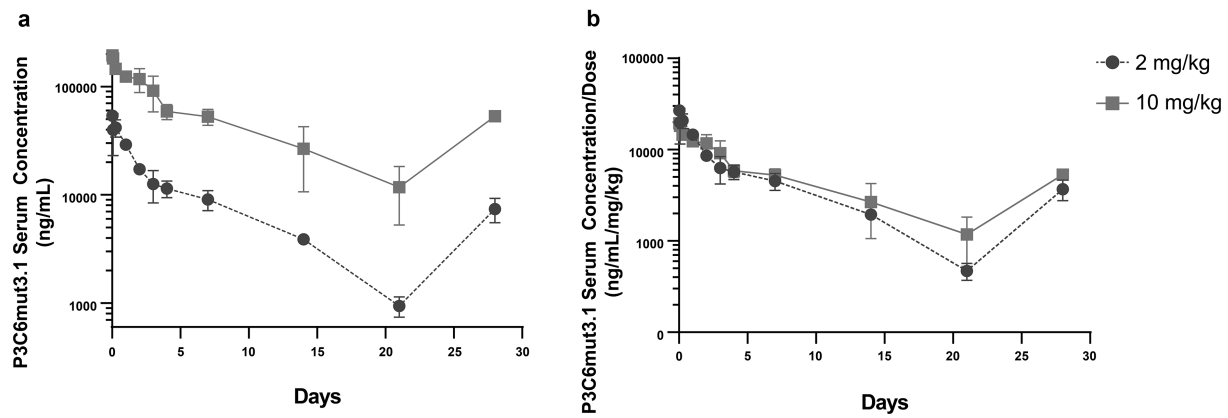


Figure 8. Pharmacokinetics of full-length IgG_{D/B} P3C6mut3.1 in healthy dogs. Healthy dogs were administered P3C6mut3.1 IgG_{D/B} intravenously at either 2 mg/kg ($n = 2$) or 10 mg/kg ($n = 2$) on Day 0 and Day 21. Blood samples were taken at the indicated time points and analyzed for the presence of P3C6mut3.1 IgG_{D/B} in the serum using a custom Meso Scale Discovery immunoassay. A. Serum pharmacokinetics of P3C6mut3.1 IgG_{D/B} with data represented as mean \pm SD. B. Dose-normalized concentration vs. time profiles for P3C6mut3.1 IgG_{D/B}.

Table 1. A non-compartmental analysis of full-length P3C6mut3.1 IgG_{D/B} PK parameters following the first dose. C_{max} : maximum observed serum concentration, AUC_{last} : area under the serum concentration vs. time curve from time 0 to 21 days, AUC_{inf} : area under the serum concentration vs. time curve extrapolated to time infinity, $t_{1/2}$: terminal log-linear half-life, CL: clearance, V_{ss} : volume of distribution.

Dose	Dog	C_{max} (ng/mL)	AUC_{last} (ng/mL*d)	AUC_{inf} (ng/mL*d)	% Extrapolated	$t_{1/2}$ (days)	CL (mL/d/kg)	V_{ss} (mL/kg)
2 mg/kg	1	5.06×10^4	1.75×10^5	1.81×10^5	2.97	4.66	11.1	69.3
	2	5.68×10^4	1.83×10^5	1.90×10^5	3.89	4.76	10.5	63.2
	Mean	5.37×10^4	1.79×10^5	1.85×10^5	3.43	4.71	10.8	66.2
	SD	4.3×10^3	5.3×10^3	6.8×10^3	0.65	0.07	0.4	4.4
10 mg/kg	3	1.84×10^5	9.57×10^5	1.01×10^6	5.45	5.33	9.88	66.4
	4	2.04×10^5	1.08×10^6	1.32×10^6	18.2	10.2	7.57	92.7
	Mean	1.94×10^5	1.02×10^6	1.17×10^6	11.8	7.75	8.72	79.6
	SD	1.4×10^4	8.8×10^4	2.19×10^5	9.0	3.42	1.64	18.6

elimination rate increasing as concentrations decrease. Additionally, the dose-normalized PK profiles (Figure 8B) showed a lack of superimposition at later time points, further suggesting a non-linear PK. Based on these data, the Highest Non-Severely Toxic Dose (HNSTD) tested was 10 mg/kg and the MTD was not defined. The No Observed Adverse Effect Level (NOAEL) was 10 mg/kg. Although anti-drug antibodies (ADA) were not measured in this study, due to the lack of a validated ADA assay, a sharp decline in drug concentrations was not observed after the first or second dose of P3C6mut3.1 and similar drug concentrations were identified in the serum on Day 28 (7 days post dose 2) and Day 7 which suggests that ADA is not accelerating antibody elimination on the second dose. Thus, the PK data are consistent with the lack of impact of ADA over this time period.

Discussion

The use of checkpoint inhibitors in veterinary medicine is in its infancy, mostly due to the lack of available, validated, fully canine monoclonal antibodies that can be safely administered to canine patients. However, the increasing recognition of companion animals with spontaneous diseases, including cancer, as a valuable parallel patient population to expedite human therapeutic advances has driven the need to generate biosimilars that can be employed in the dog to explore correlative biomarkers of response and tolerability and efficacy of combination therapies. Furthermore, there is an intense drive by pet

owners for comparable human therapies to be made available to the veterinarian to safely and effectively improve clinical outcomes. The generation of a fully canine anti-cPD-1 antibody now enables such studies to be explored.

As of August 2022, 14 FDA/EMA-approved therapeutic antibodies have been developed using phage display, including the world's bestselling antibody, adalimumab.²⁴ The technology provides a rapid method to isolate numerous unique scFvs that can be screened for desired functional and developability characteristics to identify lead candidates to move to a clinical setting. Furthermore, as the phenotype and genotype of each scFv are linked within the phage, the VH and VL nucleotide sequences encoding the desired scFv can be rapidly determined and used to generate alternative antibody-based formats including bi-specific T cell engagers, bi-specific antibodies, and chimeric antigen receptor constructs that can be tested. Competing technologies in the veterinary space include the generation of chimeric antibodies in which the VH and VL sequences of cross-reactive human or murine antibodies are assembled with a canine Fc domain or "caninization" of either human or mouse antibodies where complementarity determining regions (CDRs) are grafted onto canine antibody framework regions. Several groups have previously generated chimeric rat/dog or caninized anti-cPD-1 antibodies and evaluated them in small pilot clinical trials in dogs with different tumor histologies including oral malignant melanoma.^{25,26} As with human anti-PD-1 therapies, treatment related adverse events

including low-grade fever and gastrointestinal side effects were seen in 19/30 cases (63.3%). One death occurred secondary to pneumonitis following the administration of the chimeric rat/dog antibody. A case of steroid-responsive transaminitis was also identified in this cohort. In contrast to the chimeric antibody, no treatment-related adverse events greater than grade 3 were observed with the caninized antibody. Modest clinical responses were observed with 8/24 dogs with oral malignant melanoma experiencing either a partial response (4/24) or stable disease (4/24). However, chimeric and caninization technologies are limited by the availability of cross-reactive human or murine antibodies as well as their potential to induce anti-drug antibodies which can adversely affect antibody PK upon subsequent administrations. Additional technologies such as immunizing canines with the target antigen of interest and subsequently cloning VH and VL chains from B cells are restricted in their ability to produce high-affinity antibodies by the laws of central tolerance. Advanced technologies that involve genetic engineering of mice to house the canine immunoglobulin locus such that immunization leads to the generation of canine antibodies have been generated but have yet to be proven to encompass the full complement of canine immunoglobulin genes or to produce high-affinity antibodies for clinical development. Furthermore, the possible diversity in antibody repertoire that can be generated through the immunization of mice with canine antigens will be limited to only antigen epitope specificities that differ between the canine and murine versions of the antigen. In contrast, the selection of antibodies from phage display libraries is not subject to such *in vivo* tolerance mechanisms.

Predictive biomarkers of response to checkpoint inhibition are actively being pursued. One such biomarker that has shown correlation with objective response rates is tumor mutational burden (the number of non-synonymous somatic mutations per Mb within the tumor).²⁷ This is exemplified by the identification of positive responses to anti-PD-1 therapy in human patients with colorectal cancer with high microsatellite instability and/or mismatch repair deficiency (MSI-H/MMRd) compared to those with colorectal cancer that have low MSI and proficient MMR mechanisms.^{28,29} In general, the TMB of canine cancers is lower than that of adult human cancers and more comparable with pediatric cancer counterparts.¹⁰ In dogs, as in humans, TMB varies with tumor type, with oral melanoma, T cell lymphoma, osteosarcoma, and hemangiosarcoma having a higher TMB and mammary carcinomas, glioma and B cell lymphoma having a lower TMB. Since MSI-H/dMMR status can be readily assessed via PCR, this together with targeted sequencing panels may be of value in stratifying canine patients to checkpoint inhibitor trials and therapies. Further, the advent of gene expression profiling by bulk and single-cell RNAseq or targeted gene expression panels and antibodies that recognize potential biomarkers such as cPD-1 and cPD-L1 by flow cytometry or IHC now enables a more in-depth analysis of canine immune responses including checkpoint ligand expression and provides a means to evaluate correlative biomarkers of response. As such, the tools are now in place to leverage

canine cancer patients to better understand responses or lack thereof to ICI therapy, and this may be valuable in informing future human clinical trial designs.

Previous studies have demonstrated that human CAR-T cells isolated from solid tumors are hypofunctional and that expression of checkpoints such as PD-1, Lag-3, and TIM-3 contribute to this hypofunctionality.³⁰ Interestingly, the use of pembrolizumab in human patients with B cell lymphomas who had failed CD19 CAR-T cell therapy produced clinical benefit in 33% of the patients (4/12), and the use of pembrolizumab was associated with an increase in CAR-T activation and proliferation and less exhaustion.³¹ Favorable results associated with PD-1 blockade delivered up to 17 weeks post-mesothelin CAR-T therapy were also observed in a phase I study in human patients, contributing to the call for additional studies to evaluate the combination of anti-PD-1 antibodies with adoptive cellular therapies.³² The results reported here indicate similar findings, where P3C6mut3.1 was able to reverse the effects of cPD-L1 mediated suppression on canine CAR-T proliferation and degranulation. The development of a fully canine, validated anti-cPD-1 antibody now sets the stage for further exploration of the effects of combination anti-cPD-1 and CAR-T cell therapy, as well as combination anti-cPD-1 and anti-CTLA4 antibody therapy and the identification of biomarkers of therapeutic response in immune competent, companion dogs with spontaneous cancers.¹⁷

Evaluation of P3C6mut3.1 *in vivo* demonstrated the safety of administration by slow intravenous push, without the need for pre-medications to prevent infusion reactions. Serum pharmacokinetic data suggested that a dosing interval of no more than 2 weeks would be required to obtain target exposures. From multiple dose simulations from the PK model using P3C6mut3.1 IgG_{D/B} at 10 mg/kg every 2 weeks, exposures were obtained that matched those with nivolumab in human patients administered 3 mg/kg every 2 weeks. However, the use of receptor occupancy (RO), an important pharmacodynamic biomarker for anti-PD-1 antibodies in the human clinic, might be more informative for determining dosing scheduling. RO is measured by flow cytometry and provides a direct assessment of the degree of PD-1 engagement on the surface of activated CD4 and CD8 T cells.³³ Previous studies have shown that complete RO can be achieved using anti-PD-1 antibodies, and these assays might be useful to inform optimal antibody concentration and dosing interval and determine pharmacokinetic–pharmacodynamic relationships *in vivo*. Indeed, in clinical trials using nivolumab, peripheral RO was saturated at doses ≥ 0.3 mg/kg and ranged from 60% to 80% at 8 weeks post dosing.³⁴ Furthermore, it is acknowledged that there is a lack of optimization of clinical dosing regimens of checkpoint inhibitors in the human clinic, and provision of a comparable biosimilar may allow findings from canine dose and regimen optimization studies to guide the use of anti-PD-1 antibodies in the human arena.^{35,36} RO of P3C6mut3.1 IgG_{D/B} will be evaluated in future clinical studies in the dog, and RO-based dosing schedules may extend the dosing interval.

Here, a fully canine anti-cPD-1 antibody is described that binds with high affinity to cPD-1, effectively inhibits

cPD-1:cPD-L1 interaction and reverses the effect of cPD-L1-mediated inhibition on antigen-specific canine T cell responses. This antibody may serve as a valuable biosimilar to anti-human PD-1 antibodies to investigate correlative biomarkers of response to mono- or combination ICI and identify optimal combination regimens to inform human clinical trial design. Furthermore, P3C6mut3.1 IgG_{D/B} may prove to be a valuable addition to the veterinary armamentarium to improve the outcome of dogs with different cancer histologies.

Materials and methods

Cells and cell lines

Peripheral blood mononuclear cells (PBMCs) were isolated from the blood of healthy donor dogs (University of Pennsylvania IACUC# 807025) by Ficoll density gradient centrifugation. Cells were washed twice in complete (c)RPMI media containing RPMI 1640 with 2 mM L-Glutamine (Corning/Mediatech), 10% heat-inactivated fetal bovine serum (Atlanta Biologicals, S11150), 10 mM HEPES (ThermoFisher Scientific/Gibco), and 100 U/ml penicillin and 100 µg/ml streptomycin (ThermoFisher Scientific/Gibco) prior to use. Human cell lines (K562 and 293T cells) were grown in (c)RPMI supplemented with 1 mM sodium pyruvate (Corning/Mediatech) and 30 µg/mL gentamicin (ThermoFisher Scientific/Gibco).

cPD-1 and cPD-L1 target cell line generation

Full-length cPD-1 was amplified from cPBMC cDNA by RT-PCR, and the resulting 867-bp amplicon was cloned into the pMX-puromycin retroviral expression vector (Cell Biolabs Inc.). For cPD-L1, the 870-bp full-length sequence was synthesized and cloned into the pMX-puromycin retroviral expression vector by Genewiz (South Plainfield, New Jersey). Retrovirus was generated and used to stably transduce the human erythroleukemic K562 cell line, previously edited using CRISPR/Cas9 to remove FcγRII (KTδ32) and reduce nonspecific mAb binding, with cPD-1. Transduced cells were selected in 2.5 µg/ml of puromycin dihydrochloride (Sigma-Aldrich) to yield KTδ32-cPD-1. Expression of cell surface cPD-1 was confirmed by flow cytometry. For cPD-L1 expressing target cells, K562 expressing canine CD20 (K562-cCD20) were generated as previously described³⁷ and both wild-type K562 cells and K562-cCD20 cells were transduced with cPD-L1 to generate K562-cPD-L1 and K562-cCD20-cPD-L1 cells, respectively. K562-cPD-L1 and K562-cCD20-cPD-L1 cells were bulk sorted by flow cytometry based on PD-L1 expression, and clones were expanded in supplemented (c)RPMI as described above.

scFv phage ELISA

For ELISAs to detect binding of phage-displayed scFvs, microplate wells were coated with cPD-1 protein (Recombinant; His Tag) (Sino Biological 70,109-D08H) and human CD19 (Sino

Biological 11,880-H08H), canine CD19 (Sino Biological 70,079-D08H), or canine IL-13 Rα2-Fc (Sino Biological 11,350-H03H) as control antigens as previously described for phage display library panning.^{17,19} Briefly, polyclonal phage from the PEG-concentrated initial phage library (P0) and antigen enriched libraries obtained after each round of panning (P1 through P4) or monoclonal phage prepared from randomly picked phage clones from output plates of the third round (P3) and fourth round (P4) of panning were added to recombinant cPD-1 coated wells. After 1-h incubation at 37°C, plates were washed with 0.1% Tween 20 in phosphate-buffered saline (PBS) and horseradish peroxidase (HRP)-conjugated anti-M13 mAb (Sino Biological 11,973-MM05T-H) diluted 1:5000 in MPBS was added. Plates were washed again, and a bound HRP-conjugated secondary antibody was detected with ABTS. OD was read at 405 nm after 30 min using a Molecular Devices SpectraMax 340 spectrophotometer.

Soluble scFv production

Briefly, the non-suppressor TOP10F' Chemically Competent *E. coli* strain (ThermoFisher Scientific/Invitrogen, C303003) was infected with phage clones that were confirmed to bind to streptavidin immobilized and biotinylated avi-tagged cPD-1 soluble protein (Sino Biological 70,109-D27H-B) by phage ELISA. Bacterial colonies were used to start expression cultures that were induced by 0.5 mM IPTG as previously described.³⁸ Periplasmic extracts were taken from induced cultures, and His-tagged scFvs were purified by metal affinity chromatography using Ni-NTA agarose columns as previously described.³⁸

Soluble scFv ELISA

Streptavidin was coated onto 96-well ELISA plates at 30 µg/mL and incubated overnight at 4°C. Wells were blocked with 5% milk/PBST. 0.1–30 pmol of biotinylated cPD-1 protein was added to each well and incubated for 1 h at RT. 0.25 µg/ml of soluble scFvs in PBST were added to each well and incubated for 2 hr at RT. The wells were washed twice, and bound scFvs were detected using 0.5 µg/mL (1:2000 dilution) of AP-conjugated anti-HA antibody (Sigma-Aldrich, A5477). Plates were incubated for 1 h at RT. Plates were washed again, and bound scFvs were detected using Quanti-BlueTM AP colorimetric substrate (InvivoGen). Plates were read at 1 hr at OD 650 nm.

cPD-1:cPD-L1 ELISA based inhibition assay

Streptavidin (30 µg/ml) was coated onto ELISA plates and left at 4°C overnight. Streptavidin was removed, and the wells were blocked with 5% milk/PBS 0.05% Tween. In incubation volumes of 100 µl, soluble biotinylated cPD-1 (3 pmol) was incubated with 1.0, 3.0 or 10 pmol cPD-L1-Fc (Sino Biological 70,109-D02H), either alone or in the presence of selected anti-cPD-1 scFv (70 pmols) or an irrelevant scFv (against Middle Eastern Respiratory Syndrome (MERS) virus) for 1 hr on ice prior to being added to the blocked plate and incubated for 2 hr at RT. Plates were washed three

times with TBS-Tween, and cPD-L1 bound to cPD-1 was detected using an anti-Fc-AP conjugate (1:1000) (Jackson ImmunoResearch, 709-055-098). After three washes with TBS-Tween, Quanti-Blue™ AP colorimetric substrate (InvivoGen) was added for 1 h prior to spectrophotometric reading at OD 650 nm.

Full length IgG_D mAb generation

The VH and VL chains of selected scFvs were cloned into separate expression plasmids engineered to express either canine constant light kappa (InvivoGen, pfuse2-dclk), constant light lambda (InvivoGen, pfuse2-dcll), or constant IgG_D (analogous to human IgG4) heavy-chain domain (InvivoGen, pfuse-dchg4). Plasmids were transfected into 293T cells, and transformed cells were selected based on antibiotic resistance; lambda and kappa light chains were selected for using blastidicin and plasmids containing the constant IgG_D domain were selected for using zeocin.

Flow cytometric assay of soluble scFv or full-length IgG_D binding to membrane expressed cPD-1

KTδ32.cPD-1 and KTδ32 (WT) cell lines were washed twice in fluorescence-activated cell sorting (FACS) buffer (1% heat-inactivated FBS in 1X PBS with calcium and magnesium). Cells were blocked with 0.1 mg/ml of canine IgG (Jackson ImmunoResearch, 004-000-003) for 10 min at RT prior to cell surface labeling with 0.05 mg/ml of canine scFv, or 0.5 mg/ml HA-tagged P3C6mut3.1 IgG_D. After washing, an APC tagged anti-HA.11 epitope antibody (BioLegend 901,523) and viability dye 7-AAD (BioLegend 420,403) were added, and cells were incubated for 30 min at RT. Following cell surface labeling, cells were washed twice in FACS buffer and acquired on a FACS Canto II flow cytometer (BD Biosciences), and data was analyzed using FlowJo software version X (Treestar, Ashland, OR).

Functional assessment of anti-cPD-1 antibody on antigen-specific T cell activity

Canine CAR T cells were generated using a standard retroviral transduction protocol as previously described.³⁹ Briefly, negatively selected canine T cells were activated with anti-canine CD3/CD28 magnetic beads in the presence of recombinant human IL-2 (100IU/mL, Thermo Fisher Scientific/Gibco, CTP0021), IL-7 (10 ng/mL, Thermo Fisher Scientific/Gibco, PHC0071), IL-15 (10 ng/mL, Thermo Fisher Scientific/Gibco, PHC9151), and IL-21 (10 ng/mL, Thermo Fisher Scientific/Gibco, PHC0211). Two days later, cells were transduced on retronectin with a MSGV1 retroviral vector (MOI = 5) containing a canine CD20-targeted 28ζ CAR as previously described.⁴⁰ After 6 days, T cells were activated through their CAR using the K562-cCD20 cells.³⁷ Proliferation and degranulation assays were set up 6 days later.

Proliferation assay

Canine CAR T cells were labeled with 5 mM of cell trace violet (CTV) solution (ThermoFisher Scientific) in PBS according to manufacturer's instructions. Cells were washed in PBS and co-cultured with irradiated (10,000 rads) K562 target cell lines described above at an E:T ratio of 1:1. After 72-h incubation, cells were harvested, washed in FACS buffer, and labeled with biotinylated rabbit anti-mouse IgG antibody (Jackson ImmunoResearch, 315-065-003) for CAR detection. Cells were washed again twice in FACS buffer and labeled with rat anti-canine CD5 antibody (Clone: YKIX 322.3), rat anti-canine CD4 (Clone: YKIX302.9), rat anti-canine CD8 mAb (Clone: YCATE55.9, BioRad, MCA1039GA), and APC-Cy7-conjugated streptavidin (BD Biosciences 554,063) for 30 min at room temperature. Cells were washed twice in FACS buffer and fixed in 2% paraformaldehyde (Thermo Fisher Scientific). Cells were acquired on a FACS Canto II flow cytometer (BD Biosciences), and data was analyzed using FlowJo software version X (Treestar, Ashland, OR).

Degranulation assay

Canine CAR-T cells were harvested, washed, and co-cultured with irradiated target cells at an E:T of 1:1 in the presence of an anti-CD107b antibody (Clone: AC17, BioRad, MCA2558GA) (0.25 µg/mL), added at the beginning of the co-culture. Either P3C6mut3.1 or anti-MERS antibody was added to the co-culture at a concentration of 20 µg/mL. After 4-h incubation, cell suspensions were harvested, washed twice in FACS buffer, and labeled with rat anti-canine CD5 (Clone: YKIX 322.3), rat anti-canine CD4 (Clone: YKIX302.9), and rat anti-canine CD8 mAb (Clone: YCATE55.9). Following cell surface labeling, the cells were washed twice in FACS buffer and fixed in 1% paraformaldehyde. Cells were acquired on a FACS Canto II flow cytometer (BD Biosciences), and data was analyzed using FlowJo software version X (Treestar, Ashland, OR).

Canine pharmacokinetic study

Four healthy adult, intact, purpose-bred beagles (two males and two females) were acclimated for 7 days prior to P3C6mut3.1 administration. The study was performed at LFM Quality Labs, Inc. Terre Haute, Indiana, USA, and regulated under the USDA Animal Welfare Act. The protocol was reviewed and approved by LFM Quality Laboratories' IACUC. All procedures described were performed by LFM Quality Labs in accordance with LFM Quality Labs, Inc.'s standard operating procedures. No dogs were sacrificed in the performance of this study.

Dogs were randomly allocated for treatment within groups of two, blocked by age and sex. Two males and two females were listed in ascending order by age within sex. Blocks were created by placing the first two in one block and the next two in the second block. Individuals within each block were allocated to treatment by generating a random number using the

Excel RAND function. The lowest random number in each block was assigned to Treatment Group 1, and the remaining dog was assigned to Treatment Group 2. Dogs in Group 1 received P3C6mut3.1 (IgG_{D/B}) at 2 mg/kg and dogs in Group 2 received P3C6mut3.1 (IgG_{D/B}) at 10 mg/kg. These doses were based on doses of pembrolizumab evaluated in the KEYNOTE-002 study in human patients.⁴¹ All dogs received a total of two administrations of P3C6mut3.1 with an inter-dose interval of 21 days.

P3C6mut3.1 (IgG_{D/B}) was supplied as a clear, colorless solution at a concentration of 10.16 mg/ml (formulated in PBS, at pH 7.4) for this 2-group, parallel design study. The drug was administered undiluted via the cephalic vein at a constant infusion rate for all dogs of 1 mL/min over the course of 1.6 to 12.3 min depending on dog weight and dose level. No pre-medications were given. Body weights were measured and recorded at the beginning of a 7-day acclimation period (Day -7) and prior to each treatment (within 24 h of dosing). Endpoints used to determine toxicity included clinical observations, physical examinations, body temperature, body weight, food consumption, and clinical pathology (Complete Blood Count and Serum Chemistry Screen). Blood specimens were collected at selected timepoints before each dose and after drug administration. This study was non-terminal, and tissue histopathology was not evaluated.

Each dog was observed continuously throughout the entire duration of the infusion on Day 0 and Day 21 to monitor for signs of adverse events (AEs) including but not limited to lethargy, anaphylaxis, hemodynamic collapse, bradycardia, vomiting, ear flushing, urticaria, edema, or skin rashes. Blood was collected at pre-dose (within 24 h of dosing), 0.5, 2, 6, 24, 48, 72, and 96 h, and then once on Day 7 and Day 14 post-infusion ends. Blood samples were also taken pre-second dosing (on Day 20), and on Day 28. Serum samples from each timepoint were analyzed for the presence of P3C6mut3.1 (IgG_{D/B}) using a custom Meso Scale Discovery immunoassay (Charles River) for PK analysis. The dose-normalized concentration vs. time profiles for P3C6mut3.1. were calculated. Samples were also taken pre-dosing (Day -1) and on Days 7, 14, 20, and 28 for clinical pathology. General health observations were made on Days -7, 0, 1, 2, 3, 4, 7, 14, 21, and 28.

Meso Scale Discovery immunoassay for PK analysis

This assay was custom designed, validated, and performed by Charles River Discovery Services. All pre-diluted standards, quality controls, and serum samples underwent acid-dissociation. Briefly, the samples were incubated at RT for 15–25 min with 100 mM acetic acid (1:9 sample:acid) with shaking, and the acid was neutralized using 150 mM Tris. MSD streptavidin plates were blocked with 1% casein in PBS for 30 min at RT. Blocking buffer was discarded, and 2 µg/mL of biotinylated canine PD-1 was added to the plate and incubated for 1 hr at RT. The plate was washed with 0.05% Tween-20 in PBS, and 5 µg/mL of sulfo-tagged anti-dog IgG was added and incubated for 1 hr at RT. The plate was washed with 0.05% Tween-20 in PBS prior to adding 1 × MSD Read Buffer T. Plates were immediately analyzed on the SQ120 QuickPlex reader.

Abbreviations

ADA	anti-drug antibodies
AE	adverse events
AUC _{inf}	area under the serum concentration vs. time curve extrapolated to time infinity
AUC _{last}	area under the serum concentration vs. time curve from time 0 to 21 days
CAR	chimeric antigen receptor
CL	clearance
C _{max}	maximum observed serum concentration
CMS	carboxymethyl surface
cPBMCs	canine peripheral blood mononuclear cells
CTLA4	cytotoxic T lymphocyte antigen 4
CTV	cell trace violet
DCs	dendritic cells
ELISA	enzyme linked immunosorbent assay
FDA	Federal Drug Administration
GLP	good laboratory practice
HA	hemagglutinin
HIS	6x histidine tag
HNSTD	highest non severely toxic dose
IACUC	institutional animal care and use committee
ICI	immune checkpoint inhibitor
NCA	non-compartmental analysis
NOAEL	No Observed Adverse Event Level
LAG3	lymphocyte-activation gene 3
MERS	Middle Eastern Respiratory Syndrome
MFI	mean fluorescence intensity
MSI-H/MMRD	microsatellite instability-high/mis-match repair deficiency
MTD	maximum tolerated dose
PALS	periarteriolar lymphoid sheaths
PD-1	programmed cell death protein 1
PD-L1	programmed cell death ligand 1
PK	pharmacokinetics
RO	receptor occupancy
scFv	single chain variable fragment
SDS-PAGE	Sodium dodecyl-sulfate polyacrylamide gel electrophoresis
SEC-HPLC	Size exclusion-high-performance liquid chromatography
t _{1/2}	terminal log-linear half-life
TIGIT	T cell immunoreceptor with immunoglobulin and ITIM domain
TILs	tumor infiltrating lymphocytes
TIM-3	T cell immunoglobulin and mucin-domain containing-3
TMB	tumor mutational burden
TMDD	Target Mediated Drug Disposition
VH	variable heavy
VL	variable light
V _{ss}	volume of distribution

Acknowledgments

We would like to thank Joel Cassel and the Wistar Molecular Screening and Protein Expression facility for their assistance and expertise with SPR performance and analysis. We are also grateful for the support of the Penn Vet Comparative Pathology Core, which is part of the Abramson Cancer Center Support Grant (P30 CA016520); the Aperio Versa 200 scanner used for imaging was acquired through an NIH Shared Instrumentation Grant (S10 OD023465-01A1); the Leica BOND RXm instrument used for IHC and ISH was acquired through the Penn Vet IIZD Core pilot grant opportunity 2022. Special thanks to Amiko Saito Yoshimoto for assistance with high-resolution figures.

Disclosure statement

Authors NJM, DLS, HW, and MB have equity in Vetigenics LLC.

Funding

This work was supported by the V Foundation (NJM & DS), Vetigenics LLC, a generous gift from Mr. and Mrs. D. Sabey, and the NCI/SBIR under Contract 75N91018C000042 (Vetigenics LLC (NC)). SY is supported by the Japan Society for the Promotion of Science (JSPS) KAKENHI program grant numbers JP21J01155 and JP22K15018. PG is supported by NCI/NHLBI HL153696.

ORCID

Nicola J. Mason  <http://orcid.org/0000-0002-6149-4927>

References

- Freeman GJ, Long AJ, Iwai Y, Bourque K, Chernova T, Nishimura H, Fitz LJ, Malenkovich N, Okazaki T, Byrne MC, et al. Engagement of the PD-1 immunoinhibitory receptor by a novel B7 family member leads to negative regulation of lymphocyte activation. *J Exp Med*. 2000;192:1027–34. doi:10.1084/jem.192.7.1027. PMID: 11015443.
- Nishimura H, Nose M, Hiai H, Minato N, Honjo T. Development of lupus-like autoimmune diseases by disruption of the PD-1 gene encoding an ITIM motif-carrying immunoreceptor. *Immunity*. 1999;11(2):141–51. doi: 10.1016/s1074-7613(00)80089-8. PMID: 10485649.
- Spranger S, Spaepen RM, Zha Y, Williams J, Meng Y, Ha TT, Gajewski TF. Up-regulation of PD-L1, IDO, and T regs in the melanoma tumor microenvironment is driven by CD8 + T cells. *Sci Transl Med*. 2013;5(200):200ra116. doi: 10.1126/scitranslmed.3006504. PMID: 23986400.
- Betof Warner A, Palmer JS, Shoushtari AN, Goldman DA, Panageas KS, Hayes SA, Bajwa R, Momtaz P, Callahan MK, Wolchok JD, et al. Long-term outcomes and responses to retreatment in patients with melanoma treated with PD-1 blockade. *J Clin Oncol*. 2020;38:1655–63. doi:10.1200/JCO.19.01464. PMID: 32053428.
- McDermott DF, Drake CG, Sznol M, Choueiri TK, Powderly JD, Smith DC, Brahmer JR, Carvajal RD, Hammers HJ, Puzanov I, et al. Survival, durable response, and long-term safety in patients with Previously treated Advanced renal cell carcinoma receiving nivolumab. *J Clin Oncol*. 2015;33:2013–20. doi:10.1200/JCO.2014.58.1041. PMID: 25800770.
- Rosner S, Reuss JE, Forde PM. PD-1 blockade in early-stage lung cancer. *Annu Rev Med*. 2019;70(1):425–35. doi: 10.1146/annurev-med-050217-025205. PMID: 30355264.
- Jiang Y, Zhao X, Fu J, Wang H. Progress and challenges in precise treatment of tumors with PD-1/PD-L1 blockade. *Front Immunol*. 2020;11:339. doi:10.3389/fimmu.2020.00339. PMID: 32226426.
- Ayers M, Lunceford J, Nebozhyn M, Murphy E, Loboda A, Kaufman DR, Albright A, Cheng JD, Kang SP, Shankaran V, et al. IFN- γ -related mRNA profile predicts clinical response to PD-1 blockade. *J Clin Invest*. 2017;127(8):2930–40. doi:10.1172/JCI91190. PMID: 28650338.
- Balar AV, Castellano D, O'Donnell PH, Grivas P, Vuky J, Powles T, Plimack ER, Hahn NM, de Wit R, Pang L, et al. First-line pembrolizumab in cisplatin-ineligible patients with locally advanced and unresectable or metastatic urothelial cancer (KEYNOTE-052): a multicentre, single-arm, phase 2 study. *Lancet Oncol*. 2017;18:1483–92. doi:10.1016/S1470-2045(17)30616-2. PMID: 28967485.
- Alsaihati BA, Ho KL, Watson J, Feng Y, Wang T, Dobbin KK, Zhao S. Canine tumor mutational burden is correlated with TP53 mutation across tumor types and breeds. *Nat Commun*. 2021;12(1):4670. doi: 10.1038/s41467-021-24836-9. PMID: 34344882.
- Andris-Widhopf J, Steinberger P, Fuller R, Rader C, Barbas CF. Generation of antibody libraries: PCR amplification and assembly of light- and heavy-chain coding sequences. In: Barbas C, Burton DR, Scott JK, and Silverman GJ, editors. *Phage display: A Laboratory Manual*. Cold Spring Harbor, NY: Cold Spring Harbor Laboratory Press; 2001. p. 9.1.
- Manso T, Folch G, Giudicelli V, Jabado-Michaloud J, Kushwaha A, Nguefack Ngoune V, Georga M, Papadaki A, Debbagh C, Pegorier P, et al. IMGT® databases, related tools and web resources through three main axes of research and development. *Nucleic Acids Res*. 2022;50(D1):D1262–D72. doi:10.1093/nar/gkab1136. PMID: 34875068.
- Bao Y, Guo Y, Xiao S, Zhao Z. Molecular characterization of the VH repertoire in *Canis familiaris*. *Vet Immunol Immunopathol*. 2010;137:64–75. doi:10.1016/j.vetimm.2010.04.011. PMID: 20483487.
- Hwang MH, Darzentas N, Bienzle D, Moore PF, Morrison J, Keller SM. Characterization of the canine immunoglobulin heavy chain repertoire by next generation sequencing. *Vet Immunol Immunopathol*. 2018;202:181–90. doi:10.1016/j.vetimm.2018.07.002. PMID: 30078594.
- Martin J, Ponstingl H, Lefranc MP, Archer J, Sargan D, Bradley A. Comprehensive annotation and evolutionary insights into the canine (*Canis lupus familiaris*) antigen receptor loci. *Immunogenetics*. 2018;70(4):223–36. doi: 10.1007/s00251-017-1028-0. PMID: 28924718.
- Steiniger SC, Dunkle WE, Bammert GF, Wilson TL, Krishnan A, Dunham SA, Ippolito GC, Bainbridge G. Fundamental characteristics of the expressed immunoglobulin VH and VL repertoire in different canine breeds in comparison with those of humans and mice. *Mol Immunol*. 2014;59:71–78. doi:10.1016/j.molimm.2014.01.010. PMID: 24509215.
- Mason NJ, Chester N, Xiong A, Rotolo A, Wu Y, Yoshimoto S, Glassman P, Gulendran G, Siegel DL. Development of a fully canine anti-canine CTLA4 monoclonal antibody for comparative translational research in dogs with spontaneous tumors. *MABS*. 2021;13(1):2004638. doi: 10.1080/19420862.2021.2004638. PMID: 34856888.
- Rader CS, Steinberger P, Barbas CF. Selection from antibody libraries. In: Barbas C, Burton DR, Scott JK, and Silverman GJ, editors. *Phage display: A Laboratory Manual*. Cold Spring Harbor, NY: Cold Spring Harbor Laboratory Press; 2001. p. 10.1.
- Rader C, Steinberger PR, Barbas CF. Analysis of selected antibodies. In: Barbas C, Burton DR, Scott JK, and Silverman GJ, editors. *Phage display: A Laboratory Manual*. Cold Spring Harbor, NY: Cold Spring Harbor Laboratory Press; 2001. p. 11.1.
- Hong Y, Feng Y, Sun H, Zhang B, Wu H, Zhu Q, Li Y, Zhang T, Zhang Y, Cui X, et al. Tislelizumab uniquely binds to the CC' loop of PD-1 with slow-dissociated rate and complete PD-L1 blockage. *FEBS Open Bio*. 2021;11(3):782–92. doi:10.1002/2211-5463.13102. PMID: 33527708.
- Zha H, Jiang Y, Wang X, Shang J, Wang N, Yu L, Zhao W, Li Z, An J, Zhang X, et al. Non-canonical PD-1 signaling in cancer and its potential implications in clinic. *J Immunother Cancer*. 2021;9(2):e001230. doi:10.1136/jitc-2020-001230. PMID: 33593825.
- Centanni M, Moes D, Troconiz IF, Ciccolini J, van Hasselt JGC. Clinical pharmacokinetics and pharmacodynamics of immune checkpoint inhibitors. *Clin Pharmacokinet*. 2019;58(7):835–57. doi: 10.1007/s40262-019-00748-2. PMID: 30815848.
- Patnaik A, Kang SP, Rasco D, Papadopoulos KP, Ellassaiss-Schaap J, Beeram M, Drengler R, Chen C, Smith L, Espino G, et al. Phase I study of pembrolizumab (MK-3475; anti-PD-1 monoclonal antibody) in patients with Advanced solid tumors. *Clin Cancer Res*. 2015;21(19):4286–93. doi:10.1158/1078-0432.CCR-14-2607. PMID: 25977344.
- Andre AS, Moutinho I, Dias JNR, Aires-da-Silva F. In vivo phage display: a promising selection strategy for the improvement of

- antibody targeting and drug delivery properties. *Front Microbiol.* **2022**;13:962124. doi:10.3389/fmicb.2022.962124. PMID: 36225354.
25. Igase M, Inanaga S, Tani K, Nakaichi M, Sakai Y, Sakurai M, Kato M, Tsukui T, Mizuno T. Long-term survival of dogs with stage 4 oral malignant melanoma treated with anti-canine PD-1 therapeutic antibody: a follow-up case report. *Vet Comp Oncol.* **2022**;20:901–05. doi:10.1111/vco.12829. PMID: 35535636.
 26. Igase M, Nemoto Y, Itamoto K, Tani K, Nakaichi M, Sakurai M, Sakai Y, Noguchi S, Kato M, Tsukui T, et al. A pilot clinical study of the therapeutic antibody against canine PD-1 for advanced spontaneous cancers in dogs. *Sci Rep.* **2020**;10(1):18311. doi:10.1038/s41598-020-75533-4. PMID: 33110170.
 27. Yarchoan M, Hopkins A, Jaffee EM. Tumor mutational burden and response rate to PD-1 inhibition. *N Engl J Med.* **2017**;377(25):2500–01. doi:10.1056/NEJMc1713444. PMID: 29262275.
 28. Andre T, Shiu KK, Kim TW, Jensen BV, Jensen LH, Punt C, Smith D, Garcia-Carbonero R, Benavides M, Gibbs P, et al. Pembrolizumab in Microsatellite-Instability-High Advanced Colorectal Cancer. *N Engl J Med.* **2020**;383(23):2207–18. doi:10.1056/NEJMoa2017699. PMID: 33264544.
 29. Oliveira AF, Bretes L, Furtado I. Review of PD-1/PD-L1 inhibitors in metastatic dMMr/MSI-H colorectal cancer. *Front Oncol.* **2019**;9:396. doi:10.3389/fonc.2019.00396. PMID: 31139574.
 30. Moon EK, Wang LC, Dolfi DV, Wilson CB, Ranganathan R, Sun J, Kapoor V, Scholler J, Pure E, Milone MC, et al. Multifactorial T-cell hypofunction that is reversible can limit the efficacy of chimeric antigen receptor-transduced human T cells in solid tumors. *Clin Cancer Res.* **2014**;20(16):4262–73. doi:10.1158/1078-0432.CCR-13-2627. PMID: 24919573.
 31. Chong EA, Alanio C, Svoboda J, Nasta SD, Landsburg DJ, Lacey SF, Ruella M, Bhattacharyya S, Wherry EJ, Schuster SJ. Pembrolizumab for B-cell lymphomas relapsing after or refractory to CD19-directed CAR T-cell therapy. *Blood.* **2022**;139(7):1026–38. doi:10.1182/blood.2021012634. PMID: 34496014.
 32. Adusumilli PS, Zauderer MG, Riviere I, Solomon SB, Rusch VW, O’Cearbhaill RE, Zhu A, Cheema W, Chintala NK, Halton E, et al. A phase I trial of regional mesothelin-targeted CAR T-cell therapy in patients with malignant pleural disease, in combination with the anti-PD-1 agent Pembrolizumab. *Cancer Discov.* **2021**;11(11):2748–63. doi:10.1158/2159-8290.CD-21-0407. PMID: 34266984.
 33. Junker F, Gulati P, Wessels U, Seeber S, Stubenrauch KG, Codarri-Deak L, Markert C, Klein C, Camillo Teixeira P, Kao H. A human receptor occupancy assay to measure anti-PD-1 binding in patients with prior anti-PD-1. *Cytometry A.* **2021**;99(8):832–43. doi:10.1002/cyto.a.24334. PMID: 33704890.
 34. Agrawal S, Feng Y, Roy A, Kollia G, Lestini B. Nivolumab dose selection: challenges, opportunities, and lessons learned for cancer immunotherapy. *J Immunother Cancer.* **2016**;4(1):72. doi:10.1186/s40425-016-0177-2. PMID: 27879974.
 35. Hirsch I, Goldstein DA, Tannock IF, Butler MO, Gilbert DC. Optimizing the dose and schedule of immune checkpoint inhibitors in cancer to allow global access. *Nat Med.* **2022**;28(11):2236–37. doi:10.1038/s41591-022-02029-1. PMID: 36202999.
 36. Jiang M, Hu Y, Lin G, Chen C. Dosing regimens of immune checkpoint inhibitors: attempts at lower dose, less frequency, shorter course. *Front Oncol.* **2022**;12:906251. doi:10.3389/fonc.2022.906251. PMID: 35795044.
 37. Panjwani MK, Smith JB, Schutsky K, Gnanandarajah J, O’Connor CM, Powell DJ Jr., Mason NJ. Feasibility and safety of RNA-transfected CD20-specific chimeric antigen receptor T cells in dogs with spontaneous B cell lymphoma. *Mol Ther.* **2016**;24:1602–14. doi:10.1038/mt.2016.146. PMID: 27401141.
 38. Elia M, Andris-Widhopf J, Fuller R, Barbas CF. Production and purification of Fab and scFv. In: Barbas C, Burton DR, Scott JK, and Silverman GJ, editors. *Phage display: A Laboratory Manual*. Cold Spring Harbor, NY: Cold Spring Harbor Laboratory Press; **2001**. p. 12.1.
 39. Rotolo A, Atherton MJ, Kasper BT, Haran KP, Mason NJ. Genetic re-direction of canine primary T cells for clinical trial use in pet dogs with spontaneous cancer. *STAR Protoc.* **2021**;2(4):100905. doi:10.1016/j.xpro.2021.100905. PMID: 34746864.
 40. Panjwani MK, Atherton MJ, MaloneyHuss MA, Haran KP, Xiong A, Gupta M, Kulikovsaya I, Lacey SF, Mason NJ. Establishing a model system for evaluating CAR T cell therapy using dogs with spontaneous diffuse large B cell lymphoma. *Oncoimmunology.* **2020**;9(1):1676615. doi:10.1080/2162402X.2019.1676615. PMID: 32002286.
 41. Ribas A, Puzanov I, Dummer R, Schadendorf D, Hamid O, Robert C, Hodi FS, Schachter J, Pavlick AC, Lewis KD, et al. Pembrolizumab versus investigator-choice chemotherapy for ipilimumab-refractory melanoma (KEYNOTE-002): a randomised, controlled, phase 2 trial. *Lancet Oncol.* **2015**;16:908–18. doi:10.1016/S1470-2045(15)00083-2. PMID: 26115796.